IOP Publishing Nanotechnology
Nanotechnology **29** (2018) 075204 (8pp) https://doi.org/10.1088/1361-6528/aaa35d

Twin photonic nanojets generated from coherent illumination of microscale sphere and cylinder

Austen Poteet, Xu A Zhang, Hironori Nagai and Chih-Hao Chang

Department of Mechanical and Aerospace Engineering, North Carolina State University, Raleigh, NC 27695, United States of America

E-mail: chichang@ncsu.edu

Received 11 September 2017, revised 19 December 2017
Accepted for publication 21 December 2017
Published 15 January 2018

Abstract

Photonic nanojets, highly focused beams of light created by planar illumination of a microsphere, have been shown to produce narrow subwavelength beams over distances of several wavelengths in the near field. In this work, we investigate the generation of twin photonic nanojets through the illumination of a microsphere or cylinder from two coherent sources with relative phase shift. Under these conditions, symmetric twin nanojets separated by an intensity null can be generated. Compared to a photonic nanojet, the twin nanojets can achieve an even smaller subwavelength beam, and have the added advantage of having more complex intensity profiles that can be controlled by multiple parameters. Using both finite-difference time-domain and Mie theory models, the width, length, and intensity enhancement factor of the nanojet geometry are found to be functions of the phase, angle offsets, and particle geometry. Such twin photonic nanojets can find applications in optical trapping, manipulation, nanolithography, and enhancement of nonlinear optical properties.

Supplementary material for this article is available online

Keywords: photonic nanojet, particle scattering, Mie theory, nanolithography

(Some figures may appear in colour only in the online journal)

1. Introduction

Photonic nanojets have been the subject of increasing research since they were first named in 2004 [1]. By illuminating a dielectric sphere or cylinder with a plane wave, a highly focused jet of light can be produced in the near field. The ability to manipulate near-field light gives the precise control necessary to operate micro and nanoscale devices beyond the limits of classical optics. Photonic nanojets have presented themselves as a novel technique to achieve high-intensity, high-focus beams with waist narrower than the diffraction limit and propagation distance of several wavelengths [1–6]. In addition to the beam geometry, the back-scattering of light near the dielectric particle is sensitive to the presence of nanometer-scale particles [6, 7]. Further refinements of the nanojets' properties have been achieved through various means including inhomogeneous particles [8–10], elliptical or oddly shaped particles [11–13], and chains of particles [14]. These jets have potential applications in many areas from imaging and particle detection for medicine to nanofabrication. Nanojets and similar phenomena have already been demonstrated for data storage [15], advanced nanolithography techniques [16–20], and trapping and detection of nanometer-scale particles [6, 21–23].

In this work, we investigate for the first time the creation and properties of twin photonic nanojets by illuminating a dielectric sphere or cylinder with two coherent incident beams offset by a small angle. When the two incident beams are exactly out of phase, the light scattering of the two beams interfere destructively, resulting in two nanojets separated by an intensity null. Such twin nanojets can achieve further reduction in the beam width when compared to an equivalent nanojet produced by a single incident beam. In addition to particle parameters, incident wavelength, and surrounding

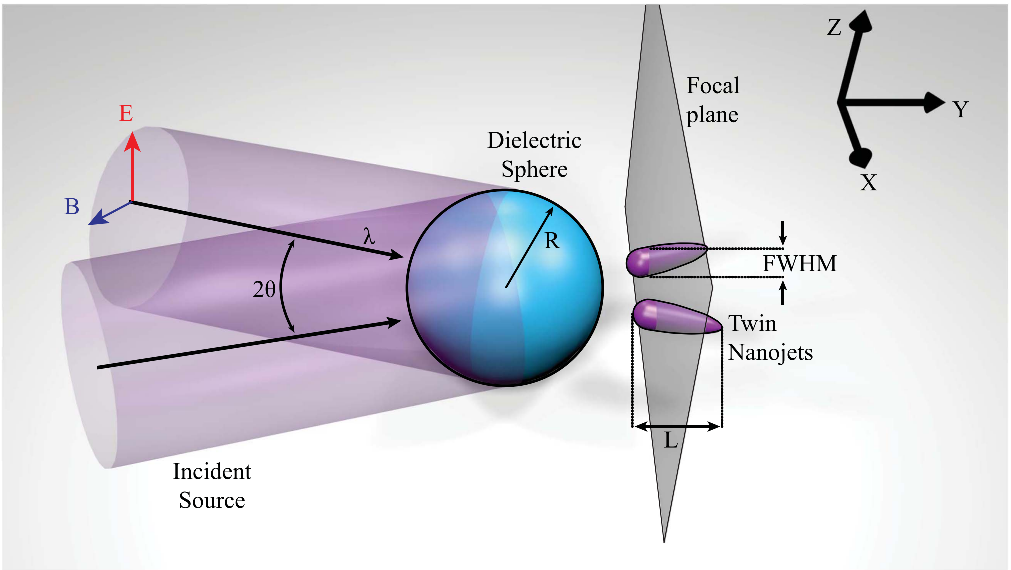

Figure 1. (a) Schematic of twin photonic nanojets generated by coherent illumination of a dielectric sphere by two plane waves. For the cylinder case the longitudinal axis is aligned along the *z*-direction.

medium, the properties of these twin photonic nanojets can also be controlled through the offset angle and relative phase shift of the incident beams. This work examines the effect of illumination conditions focusing on the beam width, length, and intensity profile of the resulting nanojets. The underlying coherent effect that is responsible for the formation of the twin photonic nanojets can also lead to super-resolution imaging of subwavelength structures [24].

2. Simulation methodology

The optical configuration is illustrated in figure 1, where a dielectric microsphere is illuminated by two mutually coherent beams in the incident xy plane. In the case of infinite cylinder, the longitudinal axis is aligned along the z-axis. Mie theory and finite-difference time-domain (FDTD) methods were both used to investigate the properties of the resulting twin photonic nanojets. In the simulation, the incident beams have wavelength $\lambda = 325$ nm and are transverse electric polarized, with the electric field aligned to the z axis. The dielectric sphere and cylinder are set to have a diameter of 10 λ. The refractive indices of the dielectric particle and surrounding medium are 1.5 and 1, respectively. The focal plane is defined here as the xz-plane located at the intensity maximum of the twin photonic nanojets.

Mie theory was used to examine the twin photonic nanojets taking advantage of the rotational symmetry of the system. This approach calculates the scattering field induced by a particle by using an eigenfunction series solution to Maxwell's equations in spherical coordinates. The external near-field amplitudes can be described as the sum of the incident field and the scattered field [25, 26]. As Mie theory has been well established as an analytical approach for modeling photonic nanojets [2, 4–6], it is ideally suited for predicting a three-dimensional field at a high resolution. Both spherical and cylindrical particle cases were calculated using Mie theory in Matlab. To apply Mie theory to multiple incident beams at an angle offset, the complex field amplitude pattern was calculated for a single, normal incidence wave. Two copies of the field patterns were rotated about the sphere's center and superimposed to find the near-field intensity resulting from both beams. A relative phase offset was added by multiplying one of the field patterns by a constant phase term before superposition. This technique allows modeling of any combination of phase and angle offset of beams while calculating only a single eigenfunction series solution to Maxwell's equations.

FDTD numerical modeling was used to further verify the results obtained from the Mie theory simulations. FDTD modeling uses Maxwell's equations discretized to the space and time partial derivatives [27], and is a useful technique for its ability to simulate complex geometries and calculate the resulting scattering patterns. Because FDTD is a finite difference approach it does not provide an exact analytical solution, but allows combinations of arbitrary geometries and multiple incident beams to be simulated. FDTD modeling was performed using the open-source software MEEP from MIT [28]. In order to accurately predict the geometries of the photonic nanojets, a mesh size of $1/100\ \lambda$ or approximately 3.25 nm was used. The incident beams were modeled as continuous sources, rather than pulses with finite duration, to approximate the response at a single wavelength. To create two oblique incident beams, a periodic boundary condition was used to match the interference fringes. Therefore the simulation domain was a multiple of the fringe period, determined by the equation: $\Lambda = \lambda/(n \sin\theta)$. Note for small angles this is generally many times the wavelength, therefore much larger than the diameter of the cylinder. As the angle of offset between the two sources, 2θ, approaches zero, the period approaches infinity. For these reasons, full three-dimensional calculations of the simulation domain at this

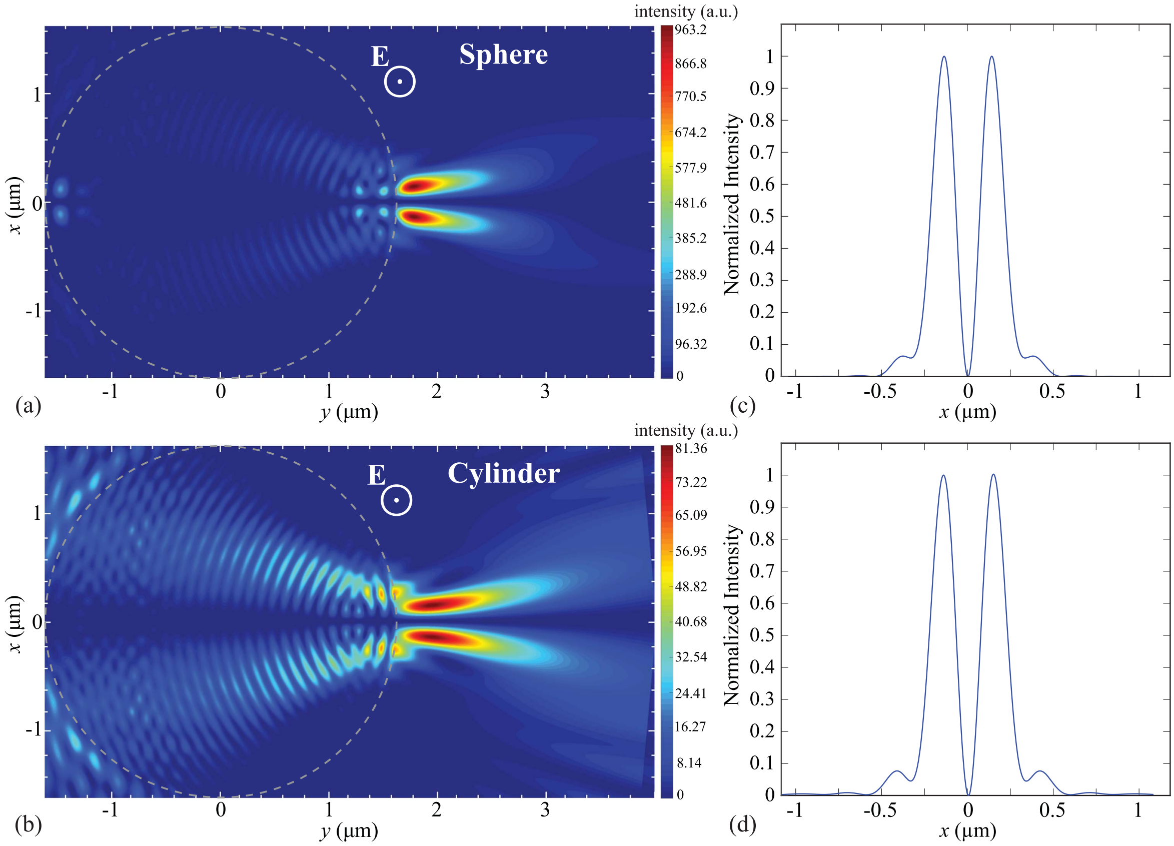

Figure 2. Intensity maps of twin photonic nanojets generated by illuminating two plane waves ($\lambda = 325$ nm) with π-phase shift and offset angle $\theta = 5°$ for dielectric (a) sphere (b) cylinder. The normalized intensity profiles at the focal plane for (c) sphere and (d) cylinder.

mesh size require excessive computational power and the FDTD method was used to only examine the 2D cylinder case for a limited range of angles.

3. Results and discussion

The intensity maps generated from Mie theory simulation for both a sphere and cylinder are shown in figure 2, and illustrate the formation of two symmetric photonic nanojets behind the dielectric particle. The particle diameters are $d = 3.25\ \mu$m with index $n_1 = 1.5$, and the ambient medium has index $n_2 = 1.0$. The intensity is defined as the full electric field squared. Here the two beams are at an offset angle of $\theta = 5°$ with π-phase offset, producing a long but focused jet in both sphere and cylinder cases. It can be observed that between the two nanojets, light interferes destructively to produce an intensity null. This creates high contrast between the center-band minimum and the two side-band maxima, as well as a slightly-lopsided shape to each jet. The normalized intensity profiles at the focal planes for the sphere and cylinder cases are depicted in figures 2(c) and (d), respectively. The full width at half maximum (FWHM) at the focal planes of the jets, roughly 150 nm–300 nm away from the edge, for sphere and infinite cylinder cases are 152 nm and 155 nm, respectively. The FWHM was calculated directly from the intensity profiles by finding the distance between the nearest points of half-maximum intensity at the focal plane. The length was defined similarly as the FWHM of the jet in the y-axis. These definitions were not changed relative to the offset angle of the incident beams. The intensity map for the cylinder case was also simulated using FDTD, and closely resembles the results from Mie theory. The x–z intensity maps at the focal planes for the single nanojet and the proposed twin nanojets using a sphere are illustrated in figure 3. While the profile of the twin photonic nanojets is drastically different from a single photonic nanojet in the x-axis, in the z-axis the properties of the jet such as FWHM remain similar to that of a comparable single photonic nanojet. Another key photonic nanojet parameter is the enhancement factor, defined as the peak intensity at the focus normalized by the incident intensity. Because the twin photonic nanojets result from two incident plane waves, each with unity amplitude, the incident intensity is four times that of a single plane wave. The enhancement factor of the twin photonic nanojets was divided by this factor of four to allow fair comparison between a single and twin photonic nanojets. The enhancement factors in figure 2 are then 240.8 and 20.3 for the sphere and cylinder, respectively. Note the enhancement factor for the twin nanojets is higher than the enhancement of 170 for a single jet generated from a sphere, as highlighted in figure 3.

The key parameters in determining the twin nanojet parameters are the angle offset and relative phase shift of the two illumination beams. This is illustrated in figure 4, where a range of angle offset for π-phase and 0-phase offsets are shown. The phase plays a dominant effect, since only a single

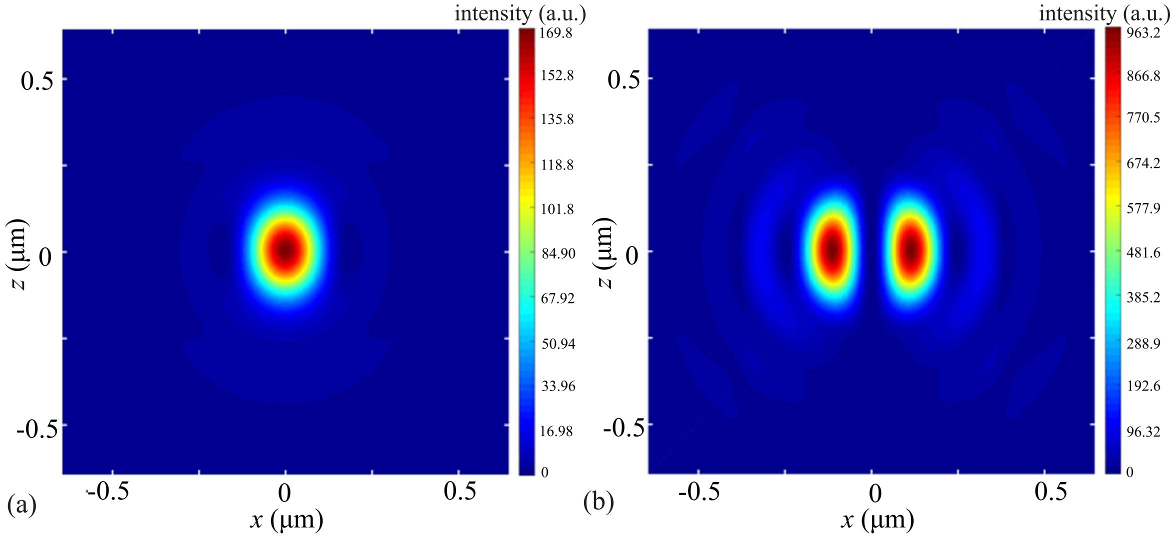

Figure 3. Intensity maps at the focal planes for (a) a single photonic nanojet, and (b) twin photonic nanojets obtained using two off-axis coherent illuminations with π-phase shift and offset angle $\theta = 5°$. These simulations are for a sphere case.

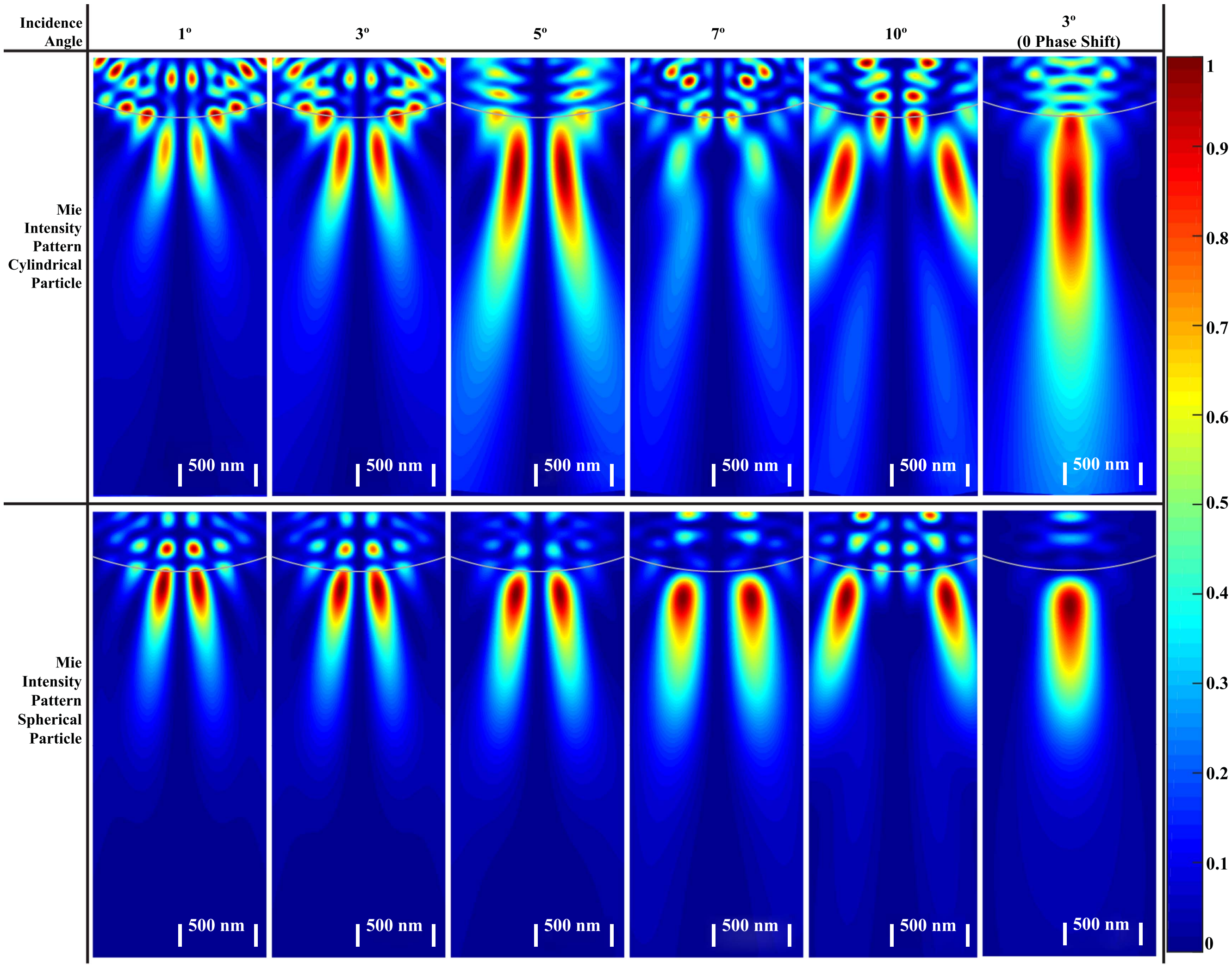

Figure 4. Matrix of selected photonic nanojet intensity patterns at offset angles 1°–10°and phase shift of π for both cylindrical and spherical particles. Photonic nanojet intensity pattern where $\theta = 3°$ at 0 phase shift shown for comparison. All intensity maps normalized to their respective maximum values.

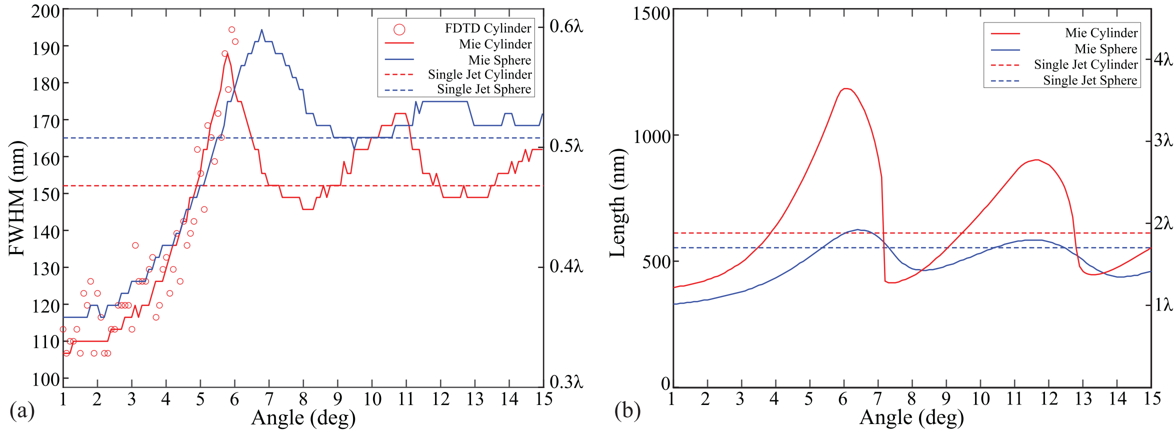

Figure 5. (a) FWHM of twin photonic nanojets as a function of offset angle. (b) Length of twin photonic nanojets as a function of offset angle.

nanojet will be obtained if the light sources are in phase, as illustrated in the right-most diagram. This is due to constructive interference, and the FWHM of the beam width would increase as a function of offset angle. When the phase is set to π, however, the destructive interference between the two sources creates the distinct twin nanojet profile. This effect is most pronounced at small angles less than 10°, as the scattering from the two incident beams overlaps and interferes. As the angle increases beyond 10°, the interference between the jets will decrease until forming two distinct jets. In this regime, the parameters of the twin nanojet approach those of the conventional single nanojet. For a range of angles between 6°–9° for the cylinder case, the interference between the jets forms smaller fringes causing the intensity profile to be indistinguishable, and clear jets do not form. This phenomenon does not appear in the sphere particle case, where the two jets diverge smoothly until becoming distinct jets. The full intensity profile evolutions from 1°–15° for cylindrical and spherical particle are presented in visualization 1 and visualization 2, respectively (see online supplementary information stacks.iop.org/NANO/29/075204/mmedia).

The FWHM, length, and enhancement factor of the twin nanojets can be compared as a function of offset angle between two beams with π-phase offset, as shown in figure 5. The parameters for a single nanojet were also simulated and plotted, and are comparable to values reported in existing literature [1, 3, 4]. The FDTD results for the cylinder case are also plotted and are in general agreement with the Mie results, however they show considerably more variance. This may be attributed to finite mesh size and rounding errors when applying the periodic boundary conditions. At an offset angle of 1°, the FWHM for both sphere and cylinder cases reach their lowest, as shown in figure 5(a). The narrowest FWHM were approximately 117 nm and 107 nm for the sphere and cylinder cases respectively, or 0.36λ and 0.33λ. This is below the FWHM of the equivalent single nanojet system, which is typically around 0.5λ. It can also be observed that below 5° offset angle, smaller FWHM can be obtained at decreasing offset angles. However, the nanojets will have lower intensity and will completely disappear as the offset angle approaches 0° due to destructive interference. At higher offset angles, the twin nanojet FWHM oscillate about the values expected for a single nanojet. The simulated length of the twin nanojets is generally comparable to a single nanojet, as shown in figure 5(b). However, it showed large oscillations with offset angle, reaching greater than 3λ between 5°–7°. Note that the staircase-like behavior seen in the FWHM plot is the result of a spatial discretization error and not the result of a physical phenomenon.

The enhancement factor of the twin nanojets, or the ratio of the intensity at the focal point to the incident beams, was also plotted versus offset angles, as illustrated in figure 6(a). Similar to the FWHM, the enhancement factor also starts low and increases with offset angle, peaking around 4° then converging to the values for a single jet. The peak enhancement is 262 and 26.7 for the sphere and cylinder cases, respectively, both roughly 50%–60% larger than those reported for a single nanojet [1, 3, 6]. At low offset angle destructive interference leads to reduction in overall intensity and a lower enhancement factor. As a result, while the twin nanojet FWHM is smaller than the single nanojet at small offset angles, the enhancement is also smaller. Therefore, there is an optimal regime between offset angles of 2.5° and 5° where both FWHM and enhancement are improved from the single-jet case.

Another unique characteristic is the intensity null between the two side-band maxima caused by destructive interference. This causes the twin nanojets to have a high intensity gradient at the center band. Figure 6(b) depicts the calculated gradient of the normalized intensity at the focal plane versus offset angle between two beams with π-phase offset. Due to the destructive interference, the peak gradient values in the focal plane are enhanced at low offset angles between the incident beams. This is attributed to smaller features, which leads to a higher local slope near the intensity null. The high intensity gradient near the center band intensity null and its tunability based on offset angle may be useful for focusing, trapping, and lithography applications.

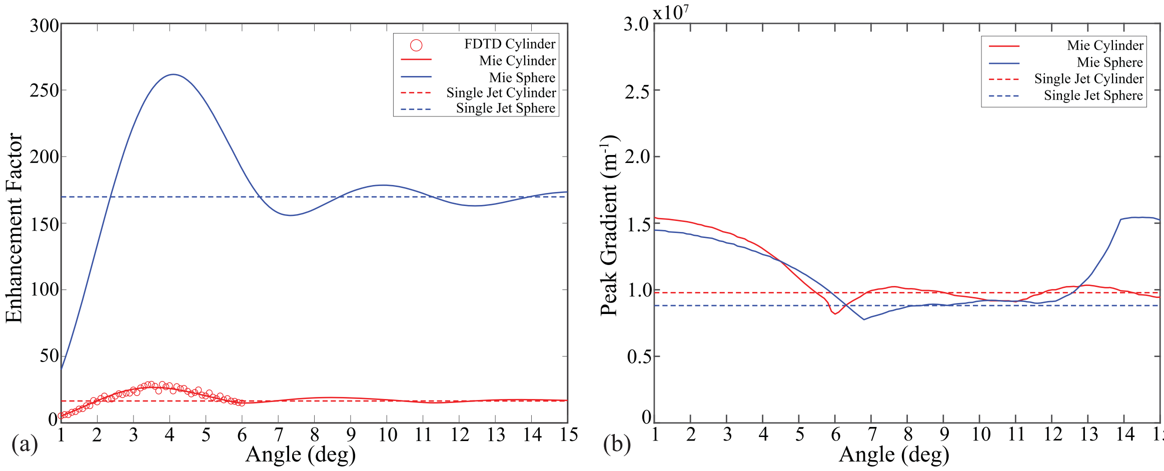

Figure 6. (a) Enhancement factor of twin photonic nanojets as a function of offset angle. (b) Peak gradient of twin photonic nanojets as a function of offset angle.

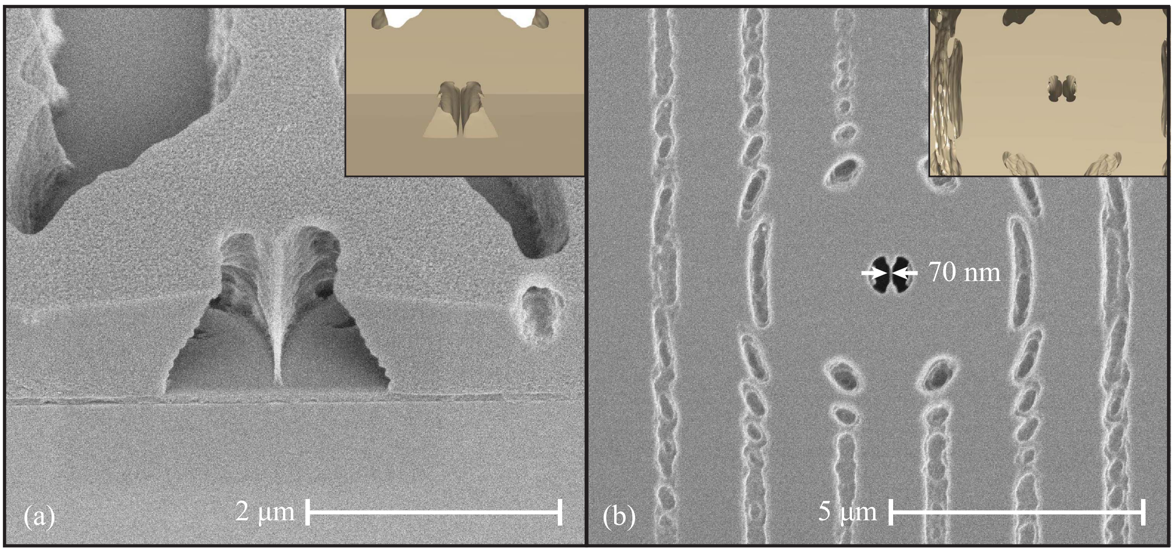

Figure 7. Lithographic impression of twin photonic nanojets produced by Lloyd's mirror interference lithography. (a) 45° angle view of twin photonic nanojet pattern with 40 mJ cm^{-2} exposure dose, (b) top view of the twin photonic nanojet pattern with 20 mJ cm^{-2} exposure dose. Inner wall is measured as 70 nm width.

4. Experimental results

To provide a physical point of reference to compare the predicted trends, an experiment was performed to visualize the twin nanojets in the near field. Here an isolated microsphere with diameter of 3 μm was placed on top of a thick positive photoresist, and a Lloyd's mirror interferometer with $\lambda = 325$ nm was used to perform the coherent two-beam exposure. A more detailed description of the experimental setup can be read in prior work [19]. The cross-section and top-view scanning electron micrographs are shown in figure 7. Here a hole with two symmetric chambers patterned by the twin nanojets can be observed. While this method cannot accurately measure the FWHM or other geometric properties of the nanojets due to exposure dependence and threshold dosage of the photoresist, it can confirm the general structure predicted by the simulation models. In particular the narrow inner wall of around 70 nm width patterned by the intensity null between the twin jets can be observed. This is only possible due to the large intensity gradient between the intensity null at center band and the nanojets.

These numerical studies and experimental demonstrations investigate and characterize the fundamental behavior of the twin photonic nanojets. Future work will focus on the effect of continuous control of phase offset between 0 and π, which may be of use for further manipulation of the two jets independently. The optical effect of additional interfering beams out-of-plane can also produce more complex nanojet patterns. The experimental demonstration of the twin nanojets for trapping and manipulation of nano/microscale objects will also be studied. Furthermore, twin nanojets may be tailored for specific applications in lithography by adjusting the various parameters to achieve subwavelength patterning of more complex geometry.

5. Conclusion

In this work, we demonstrate twin photonic nanojets with an intensity null produced by a single dielectric particle and dual incident beams. We believe this is the first examination of such twin photonic nanojets. Using Mie theory and FDTD methods, the jet FWHM, length, enhancement factor, and intensity gradient were studied. At low offset angles the FWHM of the twin photonic nanojets is narrower than a comparable single photonic nanojet, and can also achieve a 50%–60% higher enhancement factor. These behaviors suggest the potential of this phenomenon for many of the same applications as single photonic nanojets, with two added degrees of freedom, phase and offset angle, to manipulate the resulting photonic nanojets. In addition to these properties, the configuration of twin photonic nanojets presents potentially new techniques in nanoscale manipulation. The high-gradient intensity null between the nanojets is a unique feature, and could find particular use in lithographic applications. The nearness of the twin nanojets allows trapping of multiple particles in close proximity, while manipulation of the phase and offset angle would allow independent movement of each particle.

Acknowledgments

The authors acknowledge Dr Joong-Hee Min and Mr Zhiren Luo for their assistance with sample SEM imaging. This work was performed in part at the NCSU Nanofabrication Facility (NNF) and the Analytical Instrumentation Facility (AIF), members of the North Carolina Research Triangle Nanotechnology Network (RTNN), which is supported by the National Science Foundation (Grant ECCS-1542015) as part of the National Nanotechnology Coordinated Infrastructure (NNCI). This work was supported by the NSF Faculty Early Career Development (CAREER) Program (grant CMMI#1552424).

Funding

National Science Foundation (NSF) (1552424).

ORCID iDs

Chih-Hao Chang https://orcid.org/0000-0003-4268-4108

References

[1] Chen Z, Taflove A and Backman V 2004 Photonic nanojet enhancement of backscattering of light by nanoparticles: a potential novel visible-light ultramicroscopy technique *Opt. Express* **12** 1214–20
[2] Itagi A V and Challener W A 2005 Optics of photonic nanojets *J. Opt. Soc. Am.* A **22** 2847–58
[3] Ferrand P, Wenger J, Devilez A, Pianta M, Stout B, Bonod N, Popov E and Rigneault H 2008 Direct imaging of photonic nanojets *Opt. Express* **16** 6930–40
[4] Heifetz A, Kong S-C, Sahakian A V, Taflove A and Backman V 2009 Photonic nanojets *J. Comput. Theor. Nanosci.* **6** 1979–92
[5] Lecler S, Takakura Y and Meyrueis P 2005 Properties of a three-dimensional photonic jet *Opt. Lett.* **30** 2641–3
[6] Li X, Chen Z, Taflove A and Backman V 2005 Optical analysis of nanoparticles via enhanced backscattering facilitated by 3D photonic nanojets *Opt. Express* **13** 526–33
[7] Heifetz A, Huang K, Sahakian A V, Li X, Taflove A and Backman V 2006 Experimental confirmation of backscattering enhancement induced by a photonic jet *Appl. Phys. Lett.* **89** 221118
[8] Geints Y E, Zemlyanov A A and Panina E K 2011 Photonic nanojet calculations in layered radially inhomogeneous micrometer-sized spherical particles *J. Opt. Soc. Am.* B **28** 1825–30
[9] Shen Y, Wang L V and Shen J-T 2014 Ultralong photonic nanojet formed by a two-layer dielectric microsphere *Opt. Lett.* **39** 4120–3
[10] Liu C-Y 2012 Superenhanced photonic nanojet by core–shell microcylinders *Phys. Lett.* A **376** 1856–60
[11] Liu C-Y and Chang L-J 2014 Photonic nanojet modulation by elliptical microcylinders *Optik—Int. J. Light Electron Opt.* **125** 4043–6
[12] Liu C-Y 2014 Photonic nanojet shaping of dielectric non-spherical microparticles *Physica* E **64** 23–8
[13] Jalali T and Erni D 2014 Highly confined photonic nanojet from elliptical particles *J. Mod. Opt.* **61** 1069–76
[14] Yang S and Astratov V N 2008 Photonic nanojet-induced modes in chains of size-disordered microspheres with an attenuation of only 0.08 dB per sphere *Appl. Phys. Lett.* **92** 261111
[15] Kong S-C, Sahakian A, Taflove A and Backman V 2008 Photonic nanojet-enabled optical data storage *Opt. Express* **16** 13713–9
[16] Wu W, Katsnelson A, Memis O G and Mohseni H 2007 A deep sub-wavelength process for the formation of highly uniform arrays of nanoholes and nanopillars *Nanotechnology* **18** 485302
[17] Zhang X A, Elek J and Chang C-H 2013 Three-dimensional nanolithography using light scattering from colloidal particles *ACS Nano* **7** 6212–8
[18] Zhang X A, Dai B, Xu Z and Chang C-H 2015 Sculpting asymmetric, hollow-core, three-dimensional nanostructures using colloidal particles *Small* **11** 1285–92
[19] Nagai H, Poteet A, Zhang X A and Chang C-H 2017 Three-dimensional colloidal interference lithography *Nanotechnology* **28** 125302
[20] Mcleod E and Arnold C B 2008 Subwavelength direct-write nanopatterning using optically trapped microspheres *Nat. Nanotechnol.* **3** 413–7
[21] Cui X, Erni D and Hafner C 2008 Optical forces on metallic nanoparticles induced by a photonic nanojet *Opt. Express* **16** 13560–8
[22] Li Y-C, Xin H-B, Lei H-X, Liu L-L, Li Y-Z, Zhang Y and Li B-J 2016 Manipulation and detection of single nanoparticles and biomolecules by a photonic nanojet *Light: Sci. Appl.* **5** 16176

[23] Li Y, Xin H, Liu X, Zhang Y, Lei H and Li B 2016 Trapping and detection of nanoparticles and cells using a parallel photonic nanojet array *ACS Nano* **10** 5800–8

[24] Maslov A V and Astratov V N 2016 Imaging of sub-wavelength structures radiating coherently near microspheres *Appl. Phys. Lett.* **108** 051104

[25] Bohren C F and Huffman D R 1998 *Absorption and Scattering of Light by Small Particles* (New York: Wiley)

[26] Schäfer J, Lee S-C and Kienle A 2012 Calculation of the near fields for the scattering of electromagnetic waves by multiple infinite cylinders at perpendicular incidence *J. Quant. Spectrosc. Radiat. Transfer* **113** 2113–23

[27] Taflove A and Hagness S 2000 *Computational Electrodynamics: The Finite-Difference Time-Domain Method* (Boston, MA: Artech)

[28] Oskooi A F, Roundy D, Ibanescu M, Bermel P, Joannopoulos J D and Johnson S G 2010 MEEP: a flexible free-software package for electromagnetic simulations by the FDTD method *Comput. Phys. Commun.* **181** 687–702